

## Effects of additives and sintering temperature on phase evolution and properties of carbon-clay ceramic composites

Fatai Olufemi Aramide<sup>a,b,\*</sup>, O. D. Adepoju<sup>a</sup> and Abimbola Patricia Popoola<sup>b</sup>

<sup>a</sup>Department of Metallurgical and Materials Engineering, Federal University of Technology, P.M.B. 704, Akure, Nigeria.

<sup>b</sup>Department of Chemical, Metallurgical and Materials Engineering, Tshwane University of Technology, Staatsartillerie Road, Pretoria West, South Africa

Effects of additives on phase development and physico-mechanical properties of mullite-carbon was investigated. Powdered clay, kaolinite and graphite of predetermined compositions were blended with additives using ball mill for 3 hrs at 60 rev/min. Samples were produced by uniaxial compression and sintered between 1400 °C and 1600 °C for one hr. They were characterized for various properties, developed phases and microstructural features. It was observed that the properties and phase developments in the samples were influenced by the additives. 10 wt % SiC served as nucleating point for SiC around 1400 °C. 10 wt % TiO<sub>2</sub> lead to development of 2.5 wt % TiC at 1500 °C which increased to 6.8 wt % at 1600 °C. Ifon clay in the sample leads to development of anorthite and microcline in the samples. 10 wt % TiO<sub>2</sub> is effective as anti-oxidant for graphite up to 1500 °C. Base on strength and absorbed energy, sample C (with 10 wt % TiO<sub>2</sub>) sintered at 1500 °C is considered to be optimum.

**Key words:** Additives, Ceramic composite, Carbon-clay, Phase development, Mullite.

### Introduction

Refractory ceramic materials are vital for the nascent industrial and technological developments [1, 2]. Foundry work through which metals and alloys are cast into the required shapes would have been impossible without these important materials. Various activity of heat conservation to attain high temperature will not have been possible without ceramic.

However, as important as these materials are, the monolithic ceramics are prone to catastrophic failure due to their intrinsic brittleness. This makes it a necessity to develop ceramic composites with reinforcing phases within the main matrix to impart some measure of toughness to the material [3-5].

Ceramic matrix composites belong to sub-division of engineering ceramics, in which both the matrix and the reinforcement made of ceramic materials. This concept was developed to overcome brittleness of monolithic engineering ceramics. Precisely, one of the main reasons for developing ceramic matrix composites is to improve on their mechanical properties. Moreover, these materials are employed in applications that involve elevated temperatures due to their high temperature stability and good corrosion resistance. However, the intrinsic low fracture toughness of ceramics and ceramic matrix composites make them unsuitable for some

specific applications. Several techniques have been developed to improve fracture toughness of ceramics by incorporation of additives including particles (SiC, TiO<sub>2</sub>, magnesia, alumina, etc.) and fibers (C, SiC, mullite, etc.). For illustration, it was reported that addition of SiC nanoparticles into Al<sub>2</sub>O<sub>3</sub> [6-8] altered the fracture mode of Al<sub>2</sub>O<sub>3</sub> from intergranular to transgranular. As it is known, this transition can be interpreted as improved strength and toughness in ceramics [9-11].

Many researchers have reported their findings in their effort to develop and improve the properties of ceramics [12-14]. Dong et al [15], evaluated the influence of additives like MgO, SiO<sub>2</sub>, Fe<sub>2</sub>O<sub>3</sub> and ZrO<sub>2</sub> on the mechanical and thermal properties of aluminum titanate ceramics. They drew conclusion that the combined additives of MgO and Fe<sub>2</sub>O<sub>3</sub> excellently improved on the stability of aluminum titanate. Ebadzadeh and Ghasemi [16], showed how the addition of TiO<sub>2</sub> to mullite-ZrO<sub>2</sub> composites results into change of reaction sintering, densification and microstructure which alter the formation temperature and retention of t-ZrO<sub>2</sub> phase in these composites. Moya et al. [17] stated that the microstructure of mullite-zirconia and alumina-zirconia composites can be modified by additives like CaO and MgO.

The author in collaboration with others have earlier investigated the effects of TiO<sub>2</sub> [18] and silicon carbide (SiC) [19, 20] on the mineralogical and mechanical properties of mullite-carbon ceramic composite. The samples were made of the same materials but without

\*Corresponding author:  
Tel : +2348038509288, +27813778360  
E-mail: foaramide@futa.edu.ng, AramideFO@tut.ac.za

Ifon clay. The main aim of the present work is to improve on the properties of the ceramic composite through the incorporation of the Ifon clay which mainly consists of feldspar minerals.

## Materials and Methods

### Materials

The kaolin sample was sourced from Okpella [21], Edo State, Nigeria. The Ifon clay was sourced from Ifon [22], Ondo State, Nigeria. The graphite, titania and silicon carbide produced Hopkin & Williams Ltd with purity 98.5%, 99% and 96.5%, respectively.

The Ifon clay and kaolin samples were first separately soaked in water for three days to form slurry. The slurries were then sieved to remove stones and other coarse materials. The sieved slurries were then allowed to settle down for three days after which the clear water was decanted. The dispersed fine clays in water (clay slurries) were then poured into plaster of Paris (P.O.P) molds and left undisturbed for three days in order to allow the remaining water present to drain out completely. The resulting plastic clay masses were sun dried and subsequently dried in a laboratory oven at 110 °C for 24 hrs. The resulting dried clay samples were crushed and milled in a Rawwley Sussex grinder to an average particle size of 300 µm. The powders were weighed per batch on a sensitive electronic weighing balance. The individual (batch) composition was thoroughly mixed in a ball mill for 3 hrs. at 60 rev/min. The compositions of the blended samples were shown in Table 1

The resulting homogenous powder mixtures were compacted uniaxially into samples dimensions 50 × 50 × 50 mm, using a compression pressure of 100 MPa for the various analyses.

### Sintering process

The samples were fired at varying temperatures (1400 °C, 1500 °C and 1600 °C) in an electric furnace. The rate of firing differs with increased temperature (room temperature to 500 °C the sintering rate was 25 °C/minute, 501 °C to 1000 °C the sintering rate was 10 °C/minute while above 1000 °C the sintering rate was 2 °C/minute). On reaching the various sintering temperatures, the samples were held for one hour at the temperature before the furnace was switch off and the samples were allowed to cool in the furnace. The samples were subjected to various test to examine the phase analysis, evaluate their physical and mechanical

**Table 1.** Composition of the samples.

Sample designation	Graphite (wt. %)	Kaolin (wt. %)	Ifon Clay (wt. %)	SiC (wt. %)	TiO <sub>2</sub> (wt. %)
B	30	35	25	10	0
C	30	35	25	0	10

properties.

### Testing

Archimedes method was used to determine the apparent porosity and the bulk density. The immersion liquid was water. The procedure was describe in the literature [23, 24]. While the water absorption of the samples was examined according to ASTM C373-18 standard test methods for determination of water absorption and associated properties [25].

The samples were prepared for XRD analysis using the back-loading preparation method. The samples were analysed using a PANalyticalX'Pert Pro powder diffractometer with X'Celerator detector and variable divergence- and receiving slits with Fe filtered Co-Kα radiation. The relative phase amounts in weight % were estimated using the Rietveld method (FullProf). Amorphous phases were not taken into consideration in the quantification.

The microstructure of the sintered samples was examined using ultrahigh resolution field emission scanning electron microscope (UHR-FESEM) equipped with energy dispersive spectroscopy (EDS).

The samples were prepared for metallography by series of grinding and polishing. This was followed by etching using a mixture of 40 ml sulphuric acid, 20 ml nitric acid and 10 g of KClO<sub>3</sub>. Particle images which are obtained with a secondary electron detector.

### Mechanical properties

The cold crushing strength of the sintered samples was determined by uniaxial compressive tests. The standard ceramic samples were dried in an oven at a temperature of 110 °C, allowed to cool. The cold compression strength tests were performed on INSTRON SERIES 3369 at a fixed crosshead speed of 10mm min<sup>-1</sup>. Samples were prepared according to ASTM C133-97 (ASTM C133-97, 2003) [23, 34, 26]. The cold crushing strength of standard and conditioned samples can be calculated from the equation:

$$\text{Cold Crushing Strength} = \frac{\text{(Load to fracture)}}{\text{(Cross sectional area of sample)}} \quad (1)$$

## Results and Discussion

Table 2 shows the phases in the Ifon clay sample and Fig. 1 shows the XRD pattern of the of the Ifon clay sample. From the figure, the major mineralogical phases present in Ifon clay are quartz, aluminosilicate (kaolinite, illite/muscovite, plagioclase and microcline), hematite and titania. The mineralogical contents of the kaolin and Ifon clay with some other clay deposits have been discussed in earlier publication [21, 22]. Figs. 2, and 3 respectively shows the phases in the samples B and C sintered at various temperature. Figs.



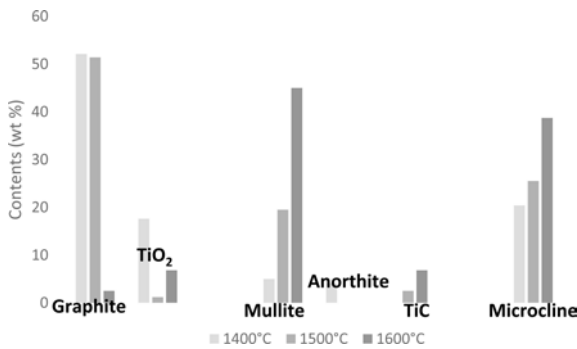


**Fig. 3.** Phases in Samples C Sintered at various temperature.

Aramide et al. 2016 [21], when the same kaolinite and graphite were used to make their samples sintered between 1300 °C and 1500 °C. They reported that less than 1 wt% of microcline and no trace of anorthite was present in the samples. This explained the origin of anorthite and microcline observed in the samples.

Table 2 and Fig. 3 show the effects of sintering temperature on the phases developed in the samples with 10 wt % titania additive (Sample C). From the figure and table it is observed that at 1400 °C the phases present in the sample are 52.1 wt % graphite, 17.6 wt % titania, 5.0 wt % mullite, 4.1 wt % anorthite and 20.4 wt % microcline. From Table 1, the raw materials from which the sample is constituted composed of 35 wt % kaolin, 25 wt % Ifon clay, 30 wt % graphite and 10 wt % titania. It is observed that the amount of graphite in sample C at sintering temperatures of 1400 °C and 1500 °C is more than those in sample B at the same temperatures. This is because of the anti-oxidation effects of titania in sample C up to 1500 °C. It could be said that titania act as anti-oxidant for the sample up to 1500 °C; beyond this temperature the graphite component of the sample is subjected to oxidation. However, as the sintering temperature of the sample is increased to 1500 °C, the graphite content is observed to slightly reduce to 51.4 wt %. Further increase in the sintering temperature leads to sharp reduction in the graphite content of the sample to 2.5 wt %.

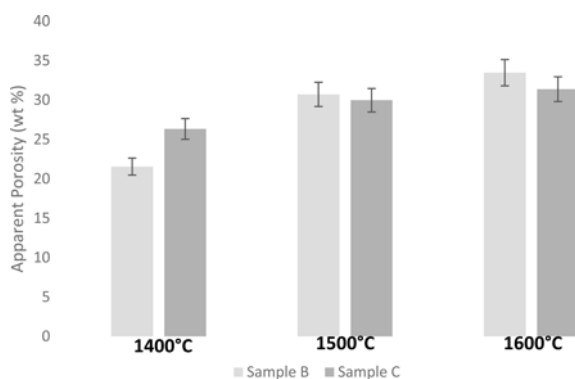
Moreover, it is observed that the sample C contained 17.6 wt % titania at 1400 °C, it however reduced drastically to 1.2 wt % as the sintering temperature is raised to 1500 °C. Further increase in the sintering resulted in the titania content being raised slightly to 6.8 wt %. On the other hand, the initial amount of mullite in the sample at 1400 °C is observed to be 5.0 wt %, it is however observed to progressively increase with increasing sintering temperature. It has a 5 wt % mullite at 1400 °C, its mullite content increases to 19.5 wt % as the sintering temperature was increased to 1500 °C, and then to 45 wt % with the sintering temperature increased to 1600 °C. Furthermore, it is observed that the initial contents of anorthite and microcline are respectively 4.1 wt % and 20.4 wt % at

1400 °C. When the sintering temperature was raised to 1500 °C the anorthite contents reduced to 0 wt % while that of microcline increased to 25.5 wt %. With further increase in the sintering temperature the amount of anorthite is maintained at 0 wt % while that if microcline further increased to 38.7 wt %. It is also observed that at 1400 °C there was no trace of titanium carbide in the sample C, but as the sintering temperature was raised to 1500 °C about 2.5 wt % titanium carbide was observed in the sample. With further increase in the sintering temperature to 1600 °C the amount of titanium carbide in the sample was observed to increase to 6.8 wt %. It can be inferred that the TiO<sub>2</sub> reacted with the carbon in the graphite at 1600 °C to form TiC. This explains why the amount of graphite in the sample reduced with the sintering temperature.

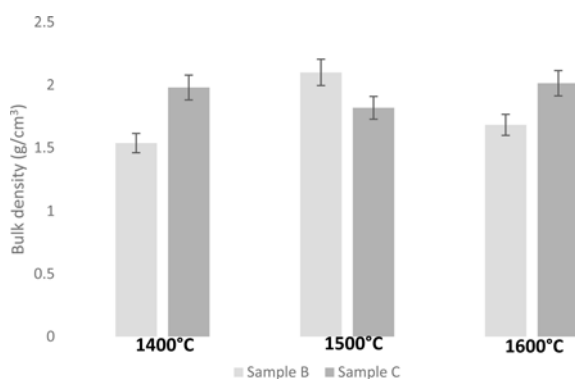
Effects of sintering temperature on the physical properties of the sintered ceramic samples

Fig. 4 shows the effects of sintering temperature on the apparent porosity of the samples B and C. From the figure, it is observed that the porosity of the samples increased with increased sintering temperature. The porosity supposed to reduce with increased sintering temperature in most ceramics due to the closure of the pores by the increasing amount of liquid phase that is developed as the sintering progresses [19]. The reason for this behavior is the reduction in the graphite content of the samples due to high temperature oxidation. Although graphite being a refractory material, is prone to high temperature oxidation at a temperature beyond 900 °C [20, 40]. Some of the graphite particles got oxidized with increased sintering temperature, leaving pores within the ceramic material, thereby increasing the apparent porosity of the samples with increased sintering temperature. It can be observed from Figure 2 that the graphite content of the sample B reduced with increased sintering temperature from 1400 °C to 1600 °C. Figure 10 shows the secondary electron images for the samples B and C. The presence of pores are seen clearly in the microstructure of the sample. For sample C the graphite content slightly reduced with increased sintering temperature from 1400 °C to 1500 °C, but sharply reduced as the sintering temperature was further raised to 1600 °C. The corresponding significant change is not observed in the porosity of the concerned sample because of the effect of silicon carbide oxidation as earlier discussed which liberates silica. The liberated silica filled some of the pores left behind by the oxidation of the carbon from graphite.

Moreover, observing the response of the porosity of the samples to the increased sintering temperature, it can be seen that even though the porosity of both samples increased with increased sintering temperature, the porosity of sample B increased more with increased sintering temperature. This is why its graphite contents at sintering temperatures of 1400 °C and 1500 °C are lower than those of sample C. It can be inferred that



**Fig. 4.** Effects of sintering temperature on the apparent porosity of the ceramic samples.



**Fig. 5.** Effects of sintering temperature on the bulk density of the ceramic samples.

sample C is more resistant to oxidation at sintering temperature range of 1400 °C and 1500 °C.

Fig. 5 shows the effects of sintering temperature on the bulk density of the sintered ceramic samples. From the figure, it can be observed that the bulk density of sample B was initially 1.54 g/cm<sup>3</sup> at 1400 °C, it increased to its maximum of 2.1 g/cm<sup>3</sup> as the sintering temperature was raised to 1500 °C, further increase in the sintering temperature of the sample to 1600 °C resulted into a reduction in the bulk density of the sample to 1.68 g/cm<sup>3</sup>. If this is compared with Fig. 4, it will be observed that the bulk density of sample B increase with increased sintering temperature from 1400 °C to 1500 °C, even though the porosity increased within the same temperature range. The reason for this is because of the effect of silicon carbide oxidation as earlier discussed which liberates silica. The liberated silica filled some of the pores left behind by the oxidation of the carbon from graphite. This is similar to what others have reported [21, 41, 42].

Alternatively, samples C followed the opposite trend to that of samples B. Its bulk density initially decreased with increased sintering temperature. The initial bulk density of sample C at 1400 °C is observed to be 1.98 g/cm<sup>3</sup>, it reduced to 1.82 g/cm<sup>3</sup> as the sintering temperature increased to 1500 °C, further increase in the sintering temperature is observed to result in the bulk density being increased to its maximum of 2.01 g/cm<sup>3</sup>. This

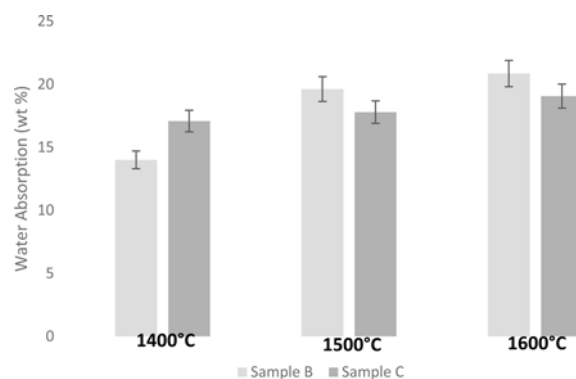


**Fig. 6.** Effects of sintering temperature on the water absorption of the ceramic samples.

could be attributed to the extra phases of TiC observed in the sample C as observed from the Table 2 and Figs. 3.

Fig. 6 shows the effects of sintering temperature on the water absorption of the sintered graphite based ceramic samples. From the figure the water absorption for sample B was 14 wt. % at the sintering temperature of 1400 °C, as the sintering temperature was raised to 1500 °C, the water absorption of the sample is observed to increase to 19.62 wt. %. Further increase in the sintering temperature to 1600 °C resulted in further increase in the water absorption of the sample

Moreover, sample C is observed to follow the same trend as sample B in the relationship of its water absorption with the sintering temperature. Its water absorption was initially 17.08 wt. % at 1400 °C, it is observed to slightly increase to 17.79 wt. % when the sintering temperature was raised to 1500 °C. Further increase in the sintering temperature is observed to lead to further increase in the water absorption of the sample to 19.06 wt. %. It will be observed that the water absorption of each of the samples follows the same trend as the apparent porosity of the corresponding sample. This is because the water absorption is directly influenced by the open pores, their structure and size.

Summarily, it could be generalized that the water absorption of all the samples increased with increased sintering temperature.

### Effects of sintering temperature and additives on the mechanical properties of the sintered ceramic samples

Fig. 7 shows the effects of sintering temperature and additives on the engineering stress of the samples being considered. From the figure it is observed that the engineering stress of sample B initially has a value of 1.67 MPa for its engineering stress at 1400 °C, it however reduced to about 0.60 MPa when the sintering temperature was raised to 1500 °C. Further increase in the sintering temperature to 1600 °C lead to the engineering stress being increased to 2.54 MPa. As earlier explained, the increase in the apparent porosity with increase in the sintering temperature has a

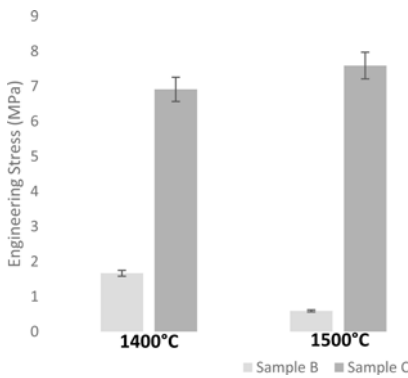


**Fig. 7.** Effects of sintering temperature on the engineering compression stress of the ceramic samples.

detrimental effect on the load bearing ability of the samples. Comparing this with the result already discussed in Fig. 4 it will be seen that increased porosity of the sample with increase in the sintering temperature reduces the load bearing ability of the sample. This agrees with the reports of other researchers [21, 41, 42], the load bearing ability of the sample B reduced with increase in the sintering temperature due to increase in the apparent porosity of the sample. Moreover, it is observed that the cold crushing strength of sample is least at 1500 °C (when it mullite fiber content is least) and that it has the highest CCS at 1600 °C (when it has the highest mullite fiber content) as revealed in Fig. 2.

Moreover, the initial value of engineering stress for sample C at 1400 °C is observed to be 6.92 MPa, it however slightly increased to about 7.58 MPa when the sintering temperature was raised to 1500 °C. Further increase in the sintering temperature of the sample to 1600 °C is observed to lead to reduction in the engineering stress of the sample to 6.12 MPa. Comparing the engineering stress of the two samples, it is observed that the engineering stress of the sample B is much lower than those of the sample C at all temperatures. Furthermore, from Fig. 3, it is has been explained that the mullite contents of the sample increased with increased sintering temperature. The presence of titania and titanium carbide could be inferred to contribute to marked difference in the CCS values of the samples B and C at all temperature. Moreover, it has been reported that titania additives substantially aids densification of compacted sintered ceramic samples [43]. This presence of titania (as sintering aid) and the relatively less pore volume in sample C may account for the marked difference in its CCS when compared to that of sample B. This can be observed from the SEM images of the samples in Figure 10.

Fig. 8 shows the effects of sintering temperature and additives on the absorbed energy of the sintered ceramic samples. From the figure it is observed that the initial absorbed energy sample B had an initial value of

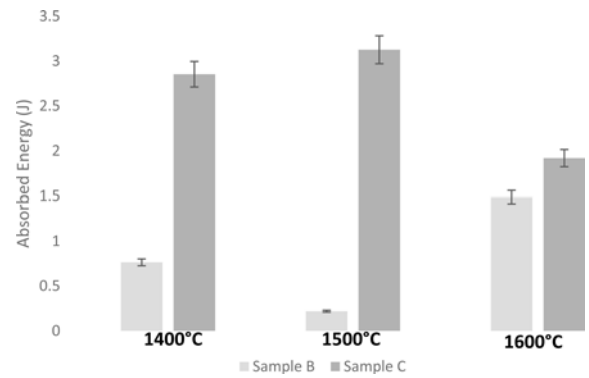


**Fig. 8.** Effects of sintering temperature on the absorbed energy of the ceramic samples.

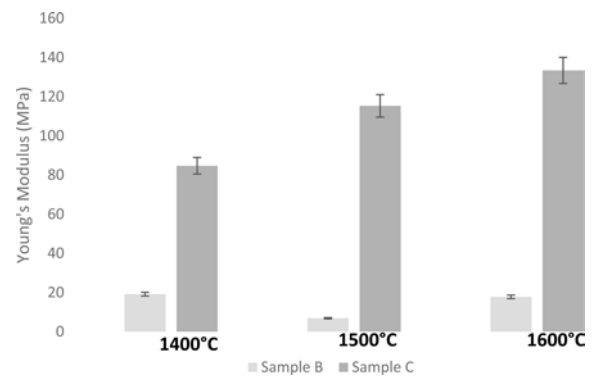


**Fig. 9.** Effects of sintering temperature on the Young's modulus of the ceramic samples.

0.76 J at 1400 °C, it is observed to reduce to a value of about 0.22 J when the sintering temperature was raised to 1500 °C. It however increased to its maximum value of 1.49 J when the sintering temperature was raised to 1600 °C.

Moreover, sample C is observed to have a value of about 2.85 J for absorbed energy at a sintering temperature of 1400 °C, it however increased to its maximum value of 3.13 J when the sintering temperature was raised to 1500 °C. Further increase in the sintering temperature is observed to result in the reduction in the absorbed energy of the sample. It will be observed that the absorbed energy of both samples followed the same trend their engineering stress followed with increased sintering temperature; it can be inferred that the absorbed energy of the samples is directly related to its engineering stress. Furthermore it is equally observed that the absorbed energy of the sample C is greater than that of sample B at all sintering temperature as it was the case for the engineering stress.

The stress-strain curves of all the sample are presented in Appendix; Figs. A2 to A7. From the figures, it can be summed that none of the samples undergone brittle failure.

Fig.e 9 shows the effects of sintering temperature and additives on the Young's modulus of the samples. It is observed that sample B at a sintering temperature of

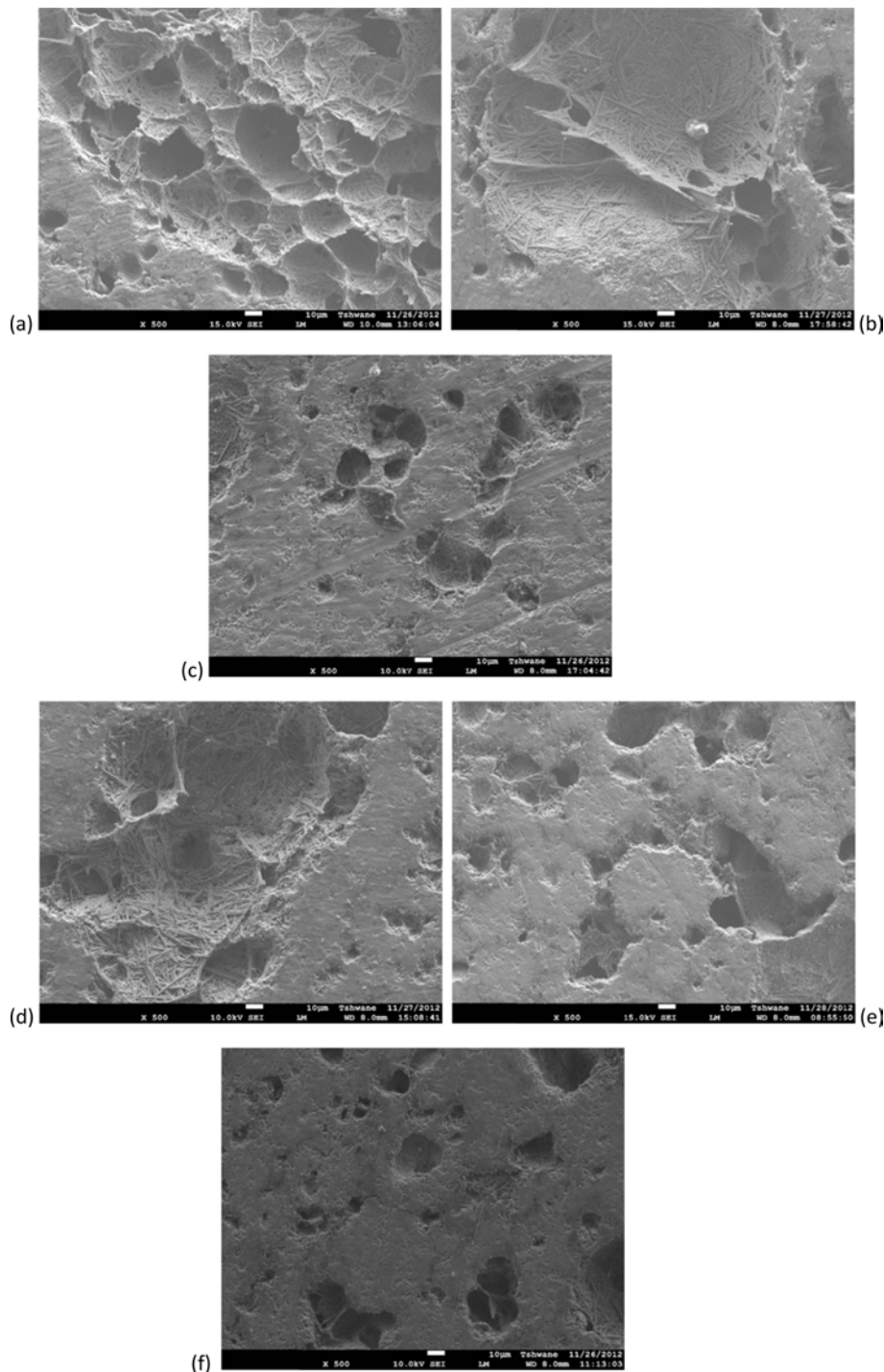


**Fig. 10.** SEM (LM mode) images of the samples: (a), (b) and (c) sample B sintered at 1400 °C, 1500 °C and 1600 °C respectively; (d), (e) and (f) sample C sintered at 1400 °C, 1500 °C and 1600 °C respectively.

1400 °C has a low value of 19.14 MPa for the Young's modulus. It further reduced to a value of about 6.88 MPa when the sintering temperature was raised to 1500 °C. Subsequently the Young's modulus of the sample is observed to increase to a value of about 17.8 MPa as the sintering temperature was raised to 1600 °C.

Moreover, the Young's modulus of elasticity of

samples C is observed to increase with increase in the sintering temperature of the ceramic samples. It is also observed that sample C has the highest values for Young's modulus at all sintering temperatures of the two samples. This could be attributed to the presence of TiC in the sample C at temperature between 1500 °C and 1600 °C.

## Conclusions

The graphite content in sample B reduces with increased sintering temperature while the graphite content of sample C is relatively stable between 1400 °C and 1500 °C but reduced with increased sintering temperature to 1600 °C. 10 wt. % SiC served as nucleus for the nucleation of SiC around 1400 °C, this lead to the formation of 50.3 wt. % SiC in the sample B at the 1400 °C. 10 wt. % TiO<sub>2</sub> in the sample C lead to the development of 2.5 wt. % TiC in the sample at 1500 °C which increased to 6.8 wt. % with increased sintering temperature. Addition of Ifon clay to sample leads to the development of anorthite and microcline in the samples B and C. The anorthite and microcline contents of sample B achieved their maxima values at 1500 °C while the microcline content of sample C increased with sintering temperature. The mullite content of the sample B slightly increased with increased sintering temperature while the mullite content of sample C increased sharply with sintering temperature. 10 wt. % TiO<sub>2</sub> is more effective as anti-oxidant for graphite between the sintering temperature of 1400 °C and 1500 °C. Based on the engineering stress and absorbed energy, sample C sintered at 1500C is considered to be optimum.

## Acknowledgments

The financial assistance of The World Academy of Science (TWAS) in collaboration with National Research Foundation (NRF) towards this research is hereby acknowledged. Opinions expressed and conclusions arrived at, are those of the author and are not necessarily to be attributed to TWAS and NRF.

## References

1. F.O. Aramide, K.K. Alaneme, P.A. Olubambi, J.O. Borode, *Int. J. of Mater. and Chem.* 5[6] (2015) 127-139.
2. F.O. Aramide and S.O. Seidu, *J. of Min. and Mater. Character. and Eng.* 1 (2013) 75-79.
3. W.D. Callister, "Materials science and engineering: an introduction" (John Wiley & Sons Inc. 2007) p. 447.
4. L. Dag and M. Annette, "Advanced Materials and Structures and their Fabrication Processes" (Narvik University College HiN, 2007) p. 55, 61
5. I.M. Low, R.D. Skala, D.S. Perera, *J. of Mater. Sc. Lett.* 13 (1994) 1334-1336.
6. A. Asadi, A.S. Vanini, A. Jabbari, *Int. J. of the Phy. Sci.* 6[22] (2011) 5253-5260.
7. A.R. Moradkhani, H.R. Baharvandi, A. Vafaeseefat, M. Tajdari, *Int. J. Adv. Design and Man. Tech.*, 5[3] (2012) 99-105.
8. N.A. Yahya, R.I. Todd, *J. Eur. Ceram. Soc.* 32 (2012) 4003-4007.
9. I. Akin, G. Goller, *Research and Innovation in Carbon Nanotube-Based Composites*, (2015) Dr. Brahim Attaf (Ed.), ISBN 978-0-9889190-1-3, WAP-AMSA.
10. I.V. Antoniac, (Ed.), *Handbook of Bioceramics and Biocomposites*, (Switzerland: Springer International Publishing, 2015) p. 54.
11. S.C. Tjong, *Carbon Nanotube Reinforced Composites Metal and Ceramic Matrices*, (Weinheim Germany: Wiley-Vch Verlag GmbH & Co, 2009) p. 45.
12. J.W. Wen-Chang, H.C. Kao, M.H. Lo, *J. Eur. Ceram. Soc.* 16 (1996) 239-247.
13. S. Maitra, S. Pal, S. Nath, A. Pandey, and R. Lodha, *Ceram. Int.* 28 (2002) 819-826.
14. N. Claussen, M. Ruhle, *Design of Transformation-Toughened Ceramics*, in *Science and Technology of Zirconia III*, *Advances in Ceramics*, vol. 24, (Am. Ceram. Soc., OH 1988) 137.
15. Dong Xiu-zhen, Wang Yi?ming, Li Yue. *J. China Ceram.* 44[1] (2008) 7-10.
16. T. Ebadzadeh, E. Ghasemi, *Ceram. Int.* 28 (2002) 447-450.
17. J.S. Moya, P. Miranzo, M.I. Osendi, *Mater. Sci. and Eng. AI09* (1989) 139-145.
18. F.O. Aramide, I.B. Akintunde, P.A. Popoola, *Acta Technica Coviniensis-Bull. of Eng.* 10[4] (2017) 121-130.
19. F.O. Aramide, I.B. Akintunde, *Acta Technica Coviniensis-Bull. of Eng.* 10[3] (2017) 99-106.
20. F.O. Aramide, I.B. Akintunde, *Leo. Elect. J. Prac. & Tech.* 16[31] (2017) 45-58.
21. F.O. Aramide, I.B. Akintunde and A. Oyetunji, *Usak University J. Mater. Sci.* (2016) 25-42.
22. F.O. Aramide, K.K. Alaneme, P.A. Olubambi, J.O. Borode, *Leo. Elect. J. Prac. & Tech.* 13[25] (2014) 46-57.
23. F.O. Aramide, K.K. Alaneme, P.A. Olubambi, J.O. Borode, *Faculty Engineering Hunedoara-Int. J. of Eng.* 7[4] (2014) 343-352.
24. F. O. Aramide, *Leonardo J. of Sc.* 14[26] (2015) 67-82.
25. ASTM C373-18 Standard Test Methods for Determination of Water Absorption and Associated Properties by Vacuum Method for Pressed Ceramic Tiles and Glass Tiles and Boil Method for Extruded Ceramic Tiles and Non-tile Fired Ceramic Whiteware Products.
26. ASTM C133-97 Standard Test Methods for Cold Crushing Strength and Modulus of Rupture of Refractories, ASTM International (2003).
27. S.K. Sadmezhaad, Z.A. Nemati, S. Mahshid, S. Hosseini, B. Hashemi, *J. Am. Ceram. Soc.* 90[2] (2007) 509-515.
28. S.K. Sadmezhaad, S. Mahshid, B. Hashemi, Z.A. Nemati, *J. Am. Ceram. Soc.* 89[4] (2006) 1308-1316.
29. Z. Nemati, S. Sadmezhaad and H.R.A. Mooghari, *Refractories Applications & News* 10[6] (2005) 17-23.
30. C.W. Forrest, P. Kennedy, J.V. Shennan, *Special Ceramics.* 5 (1972) 99.
31. P. Kennedy, "Non-Oxide Technical and Engineering Ceramics" Hampshire, S. Ed. (Elsevier, New York, 1986) 301-317.
32. G.R. Sawyer, T.F. Page, *J. Mater. Sci.* 13 (1978) 885.
33. J.N. Ness, T.F. Page, *J. Mater. Sci.* 21 (1986) 1377.
34. J. Roy, S. Chandra, S. Das, S. Maitra, *Adv. Mater. Sci.* 38 (2014) 29-39.
35. M. Auweter-Kurtz, G. Hilfer, H. Habiger, K. Yamawaki, T. Yoshinaka, H.D. Speckmann, *Acta Astronau.* 45 (1999) 93.
36. M. Panneerselvam, K.J. Rao, *Chemistry of Materials.* 15[11] (2003) 2247-2252.
37. V. Viswabaskaran, F.D. Gnanam, M. Balasubramanian, *J. Mater. Proc. Tech.* 142[1] (2003) 275-281.
38. J. She, P. Mechnich, M. Schmücker, H. Schneider, *Ceram. Int.* 27[8] (2001) 847-852.
39. K. Srikrishna, G. Thomas, R. Martinez, M. P. Corral, S.D.

- Aza, J.S. Moya, J. Mater. Sci. 25 (1990) 607-612.
40. H.Y. Zhang, H.Q. Wang, G.H. Chen, *Plastics* 35[4] (2006) 42-50.
41. F. O. Aramide, J. Min. & Mater. Character. & Eng. 11 (2012) 970-975.
42. M.I. Brasileiro, A.W.B. Rodrigues, R.R. Menezes, G.A. Neves, L.N.L. Santana, *Mater. Sci. Forum* 591-593 (2012) 117-143.
43. D. Chandra, G.C. Das, U. Sengupta, S. Maitra, *Cerâmica* 59 (2013) 487-494.